Title
Symmetry Breaking in an Edgeless Epithelium by Fat2-Regulated Microtubule Polarity

Journal
Cell Reports, 15(6)

ISSN
2639-1856

Authors
Chen, Dong-Yuan
Lipari, Katherine R
Dehghan, Yalda
et al.

Publication Date
2016-05-01

DOI
10.1016/j.celrep.2016.04.014

Symmetry-breaking in an edgeless epithelium by Fat2-regulated MT polarity

Dong-Yuan Chen[*1], Katherine R. Lipari[*1], Yalda Dehghan[1], Sebastian J. Streichan[2] and David Bilder[1**]

[1]Department of Molecular and Cell Biology
University of California, Berkeley
Berkeley, California 94720-3200 USA

[2]Kavli Institute of Theoretical Physics
University of California, Santa Barbara
Santa-Barbara, CA 93106

*Co-first authors, alphabetical order

**Corresponding Author:
David Bilder
Department of Molecular and Cell Biology
University of California, Berkeley, California 94720-3200 USA
Email: bilder@berkeley.edu
Telephone: (510)-642-8605

Running Title: PCP in edgeless epithelia

ABSTRACT

Planar cell polarity (PCP) information is a critical determinant of organ morphogenesis. While PCP in bounded epithelial sheets is increasingly well-understood, how PCP is organized in tubular and acinar tissues is not. Drosophila egg chambers (follicles) are an acinus-like 'edgeless epithelium' and exhibit a continuous, circumferential PCP that does not depend on pathways active in bounded epithelia; this follicle PCP directs formation of an ellipsoid rather than a spherical egg. Here we apply a novel imaging algorithm to 'unroll' the entire 3D tissue surface and comprehensively analyze PCP onset. This approach traces chiral symmetry-breaking to plus-end polarity of microtubules in the germarium, well before follicles form and rotate. PCP germarial microtubules provide chiral information that predicts the direction of whole-tissue rotation as soon as independent follicles form. Concordant microtubule polarity, but not microtubule alignment, requires the atypical cadherin Fat2, which acts at an early stage to translate plus-end bias into coordinated actin-mediated collective cell migration. Because microtubules are not required for PCP or migration after follicle rotation initiates, while dynamic actin and extracellular matrix are, polarized microtubules lie at the beginning of a handoff mechanism that passes early chiral PCP of the cytoskeleton to a supracellular planar polarized extracellular matrix and elongates the organ.

INTRODUCTION

Animal organs undergo development not in isolation, but in the context of global body axes that form in the early embryo. The process of planar cell polarity (PCP) allows organogenesis to occur with reference to these axes. In PCP, cells acquire a common subcellular organization within the plane of the often epithelial tissue. PCP organization involves two features: alignment with respect to a given axis, and a polarized orientation along this axis. This organization allows coordinated morphogenesis with respect to anterior-posterior, dorsal-ventral, or proximal-distal elements of the body plan (Gray et al., 2011; Wallingford, 2012; Zallen, 2007). Our understanding of PCP in morphogenesis comes almost exclusively from tissues that approximate flat sheets, and are generally treated as bounded. In paradigmatic tissues such as Drosophila wing, notum, eye and abdomen, PCP is organized by gradients of factors that specify global directional cues within the epithelium (Goodrich and Strutt, 2011; Singh and Mlodzik, 2012; Vladar et al., 2009). However, many organs contain tubular and acinar structures whose topology can be considered, in part, unbounded, and in which similarly localized sources of cartographic information may not be present. PCP around the circumference of these 'edgeless epithelia' is likely to involve distinct mechanisms of organization.

The Drosophila egg chamber (also called the follicle) is an acinar tissue that exhibits a non-canonical form of PCP (reviewed in (Bilder and Haigo, 2012; Cetera and Horne-Badovinac, 2015). This PCP is seen within the 'follicle epithelium' that encases the germline. Like paradigmatic PCP tissues, the follicle epithelium exhibits polarized cytoskeletal organization that is coordinated between cells. Basal F-actin filaments align within each follicle cell around the circumference of the tissue, perpendicular to the A-P axis. Alignment of microtubules can also be seen, as well as of fibril-like structures of extracellular matrix in the basement membrane. This organization drives a coordinated collective cell migration that leads the entire tissue to rotate circumferentially in a PCP fashion around the A-P axis. In a further parallel to many PCP tissues, follicle PCP drives A-P tissue elongation, changing shape of the growing egg chamber from an initial sphere to the distinctively ellipsoid egg. However, unlike paradigmatic PCP tissues that are polarized toward specific tissue boundaries, follicle PCP is continuous around the circumference of the tissue. Moreover, follicle PCP does not rely on Fat/Ds or Fz/Vang, the two major signaling pathways that direct PCP in bounded tissues (Bastock and Strutt, 2007; Viktorinova et al., 2009).

While mechanisms controlling tissue rotation continue to be elucidated, how PCP symmetry in the follicle is broken, and how this directs coordinated cellular motility of the tissue remains unclear. In this work we identify the earliest sign of PCP in the follicle and show that chiral polarity of MTs in the follicle precursors, rather than the follicle itself, is regulated by the atypical cadherin Fat2 and sets the template for subsequent PCP organization, tissue rotation, and organ elongation.

RESULTS

PCP rotation begins immediately following follicle budding

In order to investigate the origins of follicle PCP, we sought to examine its initial stages. Follicles form in region 3 of the germarium, where ~30 progeny of somatic stem cells residing in region 2b surround a germline cyst and establish a contiguous epithelium (**Supplemental Fig. 1)** (Nystul and Spradling, 2010). This structure, also called a stage 1 follicle, then progresses through 13 additional developmental stages to create a mature egg (Spradling, 1993). Our previous work described robust rotation at stage 5 but did not identify the time when it initiates (Haigo and Bilder, 2011). Live imaging demonstrates that follicles rotate, perpendicular to the A-P axis and with a stable chirality, shortly after they are formed (**Fig. 1A; Supplemental Movie 1**). Cetera et al., (2014) were first to report early follicle rotation, placing it at st. 1; we do not detect consistent axial movement at this stage. However, rotation was seen reliably at stage 2, after the stalk completes budding of the follicle from the germarium (**Fig. 1A-F**). We live-imaged the stage 1 to stage 2 transition and compared the timing of rotation initiation to the production of the follicle basement membrane (BM) over which the epithelial cells move. BM surrounds the stage 1 follicle at all regions except the anterior pole; BM is deposited in this region during stage 2 to isolate the follicle from the anterior stalk cells (**Fig. 1D**). Follicles in which Collagen IV (assessed by an α chain (Flybase:Vkg)-GFP fusion protein) was not detected between the epithelium and the anterior stalk did not progressively rotate, but 92% (n=12) of follicles with continuous anterior Collagen IV-GFP rotated (**Fig. 1D-F**). Once initiated, the absolute speed of rotation increased over time, from 0.2 μm/min at stage 2 to 0.5 μm/min at stage 6 (measured at the equator, **Fig. 1B**). Interestingly, while rotation speed increased, the angular velocity of rotation was much less changed, approximating 40 degrees/hour from stage 2 to stage 6 (**Fig. 1C**). As follicles rotate with a determined alignment and orientation from the time that they first become isolated from external cells, the PCP symmetry-breaking that directs rotation must originate prior to follicle formation.

Alignment of microtubules and actin precede PCP rotation

To identify the earliest molecular sign of follicle PCP, we examined the germarium, including stage 1 follicles, for proteins known to show PCP organization at later stages. An obstacle to comprehensive quantitative analysis of the germarium is its architecture. Like many tubular and acinar tissues, the germarium and early follicle have highly curved surfaces. Confocal sections of such tissues capture only the tangential fraction of the epithelial plane, while volumetric projections provide 3D visualization but not quantification along the curved surface; moreover, these approaches overrepresent the equator and miss the poles (**Fig. 2A)**. To comprehensively and accurately assess PCP in the follicle epithelium, we employed a newly-developed imaging algorithm that can accurately analyze the surfaces of contoured objects. This algorithm, ImSAnE (Imaging Surface Analysis Environment), extracts the plane of the epithelium from three-dimensional stacks and projects it two-dimensionally; projections can be chosen to maintain area or orientation, while geometric observables, generally distorted in projections, can be correctly quantified using built-in correction methods (**Fig. 2B**) (Heemskerk and Streichan, 2015). Nematic order parameters (S, see Experimental Procedures), as well as angle of orientation to axes with standard deviations can then be automatically assessed. Values for PCP elements along the entire basal surfaces of the large stage 6 follicles correspond to those previously published (**Fig. 2C**) (Cetera et al., 2014; Viktorinová and Dahmann, 2013). Using ImSAnE, we confirmed the high degree of F-actin alignment in region 2b first reported by Frydman (**Fig. 2D-F**) (Frydman and Spradling, 2001). Notably, MTs are also strongly aligned in this region, with order

parameters that parallel those of F-actin (**Fig. 2E-F**). Alignment of both actin and MTs is reduced but not lost as the follicle forms. Nematic order parameters, which are > 0.9 at stage 1, drop below 0.8 during stage 4 before recovering to 0.9 at stage 5; the standard deviation of nematic angles increases when order parameters drop. By contrast to cytoskeletal elements, we were unable to detect polarized organization of Rab10, Msn, or Ena in the germarium (Cetera et al., 2014; Lerner et al., 2013; Lewellyn et al., 2013). These data emphasize that coordinate alignment of the cytoskeleton precedes PCP rotation as well as PCP organization of several other molecular markers.

MTs are required in the germarium prior to PCP rotation

To assess the functional role of early cytoskeletal organization in follicle PCP, we employed genetic and chemical approaches. A forward genetic screen using transgenic RNAi expression specifically within the somatic gonad (unpublished results) identified several cytoskeletal regulators whose knockdown induced defects in follicle elongation. As expected from actin's well-established role in cell motility, these included regulators of actin organization. Disrupting dynamic actin by knocking down the SCAR complex regulators Hem (also known as Kette/NAP1) or Abi throughout follicle development prevents rotation and leads to round eggs (**Fig. 3E**, **Supplemental Fig. 2**) (Cetera et al., 2014; Chen et al., 2014). Sra-1 depletion had a similar effect, although it displayed a more general disruption of cortical F-actin that hindered analyses of molecular PCP. Acute chemical inhibition using the Arp2/3 inhibitor CK-666 demonstrated that Arp2/3-initiated actin polymerization is required during stages 1-5 for PCP follicle rotation (**Fig. 3E**) (Cetera et al., 2014).

Knockdown of the MT stabilizing protein CLASP (Flybase: Chromosome Bows) caused a potent loss of MT bundles, with minor effects on the formation of F-actin filaments, in both germaria and stage 1 follicles (**Fig. 3A, B**). Strikingly, CLASP-depleted follicles failed to rotate and gave rise to round follicles with mispolarized F-actin, as well as later to round eggs (**Fig. 3B-D**). Disrupting MTs by overexpressing the MT-severing protein Spastin also induced round eggs (not shown). Moreover, conditional RNAi expression revealed that CLASP knockdown after stage 3 slows but does not prevent rotation (**Fig. 3E**) and leads to only mildly round eggs (**Fig. 3F**). We confirmed these data by using chemical inhibitors. When monitoring follicles from colchicine-fed flies, we found that no stage 2 follicles initiated rotation (**Fig. 3E)**. However, follicles that were at stage 3 and later when colchicine feeding commenced continued to rotate on-axis, albeit at a slower rate (**Fig. 3E)** (Viktorinová and Dahmann, 2013). These data suggest that, while MTs are not required for cell motility driving follicle rotation per se, they are required at stage 1-2 to initiate it.

Germarial Fat2 regulates both rotation initiation and maintenance but not cytoskeletal alignment

Since MTs are required to initiate PCP follicle rotation, we considered potential regulators of germarial PCP organization. The atypical cadherin Fat2 is required to initiate rotation (Cetera et al., 2014) and for egg elongation and cytoskeletal PCP, but its role in the latter has been largely inferred from phenotypes seen ~16 hours after rotation has initiated (Viktorinova et al., 2009; 2011). We identified RNAi lines that knockdown *fat2* either strongly or mildly; the strong knockdown line phenocopies the *fat2* null phenotype with 100% penetrance (**Supplemental Fig. 3**). We examined strongly *fat2*-depleted germaria and found that they failed to rotate at stage 2, despite stalk and basement membrane morphogenesis comparable to WT, and shortly after this stage, PCP organization fails to align (**Fig. 4A-B, Supplemental Movie S2)**. To define the requirements for Fat2 in initiation and maintenance of follicle rotation, we employed

conditional knockdown, with the limitation that we were unable to directly assess the completeness of Fat2 depletion. When follicles raised at permissive conditions and initiating rotation were shifted to knockdown *fat2* at st. 3 and following, they slowed rotation within 8 hours and arrested after 12 hours; the resultant eggs showed substantial elongation defects. If *fat2* was instead knocked down prior to stage 3, follicles always failed to rotate and gave rise to round eggs, even when shifted to permissive conditions that terminated *fat2* knockdown for the remaining 40 hours of oogenesis (**Fig. 4C,D**). These results indicate an absolute requirement for Fat2 in both rotation initiation as well as maintenance, as well as elongation, following st. 2. Despite this, we found no significant changes in the circumferential alignment of either actin or MT in *fat2*-depleted or null as compared to WT germaria (**Fig. 4A, B**). Thus, Fat2 regulates rotation by a mechanism that is independent of germarial cytoskeletal alignment.

Fat2-regulated microtubule polarity in the germarium predicts follicle PCP chirality

To explore this mechanism, we took advantage of the mild *fat2* RNAi line to test genetic interactions. Knockdown of *fat2* using the mild line gives a moderately penetrant round egg phenotype: ~20% of laid eggs are round (**Fig. 4E**). This is a sensitized background, as heterozygosity for *fat2* enhances this phenotype to over 80%. Remarkably, heterozygosity for *CLASP* causes a similar degree of enhancement: over 80% of eggs laid by such females are round. This result suggests that Fat2 regulates follicle elongation through close functional ties to the MT cytoskeleton.

The intimate and essential roles of both Fat2 and MTs in initiating follicle rotation prompted us to examine early MT organization more closely. Since Fat2 did not regulate germarial MT alignment (**Fig. 4A, B**), we instead evaluated the polarized organization of the MTs. MTs have an intrinsic polarity, with a fast-growing + end and a slow-growing – end. We used the + end tracking protein EB1 to assess the polarity of the aligned MTs within live stage 1 follicles (**Fig. 4F, Supplemental Movie S3**), and calculated a bias parameter in which 0 represents unbiased MT+ end growth, while 1 represents all MT+ ends growing in the same direction. Interestingly, this analysis revealed a significant ($p<0.003$) bias in the chirality of MT + end growth, and nearly 2/3 of germaria displayed a bias of 0.2 or greater (**Fig. 4G)**. Moreover, the chirality of this MT bias was not identical in all stage 1 follicles. With respect to the ovariole A-P axis, the ratio of dextral (clockwise) to sinistral (counter-clockwise) MT +end biases seen in follicles prior to rotation was ~50%(**Fig. 4H**). This corresponds to the ratio of chiralities of rotation seen in later stage follicles (**Fig. 4H)**. To determine the relationship between MT bias at stage 1 and chirality of rotation once it initiates at stage 2, we carried out live imaging on EB1-expressing budding follicles. Of follicles that remained healthy throughout imaging, 7 of 8 showed a, germarial MT bias exceeding that of *fat2*, and 100% of these later rotated with a chirality opposite to their earlier +-end bias ($n=7$; $p<0.01$) (**Fig. 4I, Supplemental Movie S4)**. Strikingly, despite the fact that MT bundles in *fat2* mutant follicles retain PCP alignment at stage 1, their biased orientation was lost, with MT + end organization randomized (**Fig. 4G).** These results indicate that Fat2 acts in the germarium to organize MT chirality, and suggest that polarity of MT in the developing proto-follicle is the symmetry-breaking event that sets subsequent PCP including the direction of rotation after organ formation.

DISCUSSION

In this work we identify a central symmetry-breaking role for microtubule polarity in PCP of an 'edgeless' epithelial organ. MTs are the earliest PCP molecule during follicle

development, germarial MT polarity predicts the chirality of subsequent follicle PCP events, and disruption of either MT alignment or polarity in the germarium prevents all subsequent aspects of follicle PCP, including the coordinated cell motility that initiates follicle rotation. These requirements for MTs are not due to secondary effects on actin, which retains its organization in germaria with disrupted MTs. Importantly, unlike actin, which is required acutely and constantly for collective cell migration, MTs are not strictly required for follicle cell motility once rotation has initiated. We therefore propose that MTs provide the initial source of PCP information in the early follicle, and that actin, through its role in promoting tissue rotation, serves to amplify and propagate PCP.

Our data demonstrate that the MT polarity bias in the forming follicle predicts the chirality of PCP tissue rotation that initiates ~10 hours later. It was recently reported that, in st. 4 follicles, MT + end orientation anticorrelates with rotation direction at st. 7 (Viktorinová and Dahmann, 2013). However, in that work, stage 4 and earlier follicles were thought to represent pre-rotation stages, contrary to our identification here of rotation initiation at st. 2 and that of Cetera et al. (2014) who place it at st. 1. Since both MT alignment and polarity are present in the germarium, the st. 5 correlation is not predictive and reflects pre-existing PCP information rather than revealing its source. In the absence of an independent and direct manipulation of MT + end orientation, we cannot conclusively state that the MT polarity that we document in the germarium is instructive for rotational direction. Nevertheless, the strong correlation between this chirality and the subsequent direction of follicle rotation, along with disruption of both in the absence of *fat2*, point to a model in which coordination of MT polarity in cells across the follicle is required for a unidirectional consensus amongst individual motile cells to initiate productive rotation.

Our data thus suggest that the atypical cadherin Fat2, a key regulator of follicle PCP, rotation, and elongation, acts through effects on early MT polarity. Through analyses of middle stages of follicle development, it has been argued that Fat2 regulates global PCP alignment of the cytoskeleton, as does the canonical PCP regulator Fat in the developing Drosophila wing (Harumoto et al., 2010; Matis et al., 2014; Olofsson et al., 2014; Viktorinova et al., 2009; 2011). However, in *fat2* germaria, actin and MT alignment are maintained; it is coordinated MT polarity that is lost. These phenotypes, along with its strong genetic interaction with CLASP, argue that Fat2 promotes rotation initiation and follicle PCP via its effects on MT polarity. We have not excluded an additional role in actin regulation other than polarized alignment; the requirement for Fat2 and actin but not MTs to maintain rotation, as well as the direct binding of actin regulators by vertebrate Fat1, a possible ortholog of Drosophila Fat2 (Moeller et al., 2004; Tanoue and Takeichi, 2004), suggests such a role. Moreover, while this work was in revision, Squarr et al. (2016) showed that Fat2 can directly influence the actin cytoskeleton via binding to the WAVE complex.

As with PCP in the developing Drosophila wing disc (Matis et al., 2014; Olofsson et al., 2014; Shimada et al., 2006), the initial PCP bias provided by MT polarity within the early follicle precursors is mild, but becomes more robust as organogenesis progresses. A mechanism for amplification in the follicle involves whole-tissue rotation. Preventing rotation by disrupting actin or integrins causes a rapid loss of all PCP organization primed in the germarium (Bilder and Haigo, 2012; Cetera and Horne-Badovinac, 2015). Interestingly, just as MTs are largely dispensable for PCP after actin PCP becomes established (Figs. 3 and 4), actin PCP is dispensable after circumferentially aligned ECM becomes established (Cetera et al., 2014). Hence, PCP transitions from highly dynamic and intracellular MTs, to longer-lasting and sometimes juxtacellular actin filaments, and

then finally to the durable ECM fibrils that span multiple cells. PCP information in the follicle is therefore passed along by a 'handoff' mechanism, to increasingly stable as well as larger scale components that can ultimately exert force to shape the organ.

Non-centrosomal microtubule arrays, and in particular their regulated polarized organization, have previously been implicated as central governors of global PCP in tissues such as Drosophila wings, zebrafish gastrulae, and mammalian airway epithelia (reviewed in Galic and Matis, 2015; Sepich et al., 2011). In 'edged' PCP tissues in Drosophila, a 'global PCP' module molecularly controlled by Fat is thought to use gradients of positional information from specific sources to bring individual cell PCP in alignment with overall body axes (Goodrich and Strutt, 2011; Singh and Mlodzik, 2012; Vladar et al., 2009). In the circumferential 'edgeless' PCP axis of the follicle epithelium, where no such graded information is known, Fat2 seems to similarly coordinate the PCP of individual cells. That both contexts involve important roles for polarized MTs and are controlled by related protocadherins raises the possibility of ancient links between the modes of epithelial PCP organization.

Acknowledgements

We thank Christian Dahmann, Nasser Rusan, Nina Tang Sherwood and Jeff Axelrod for sending reagents, and are grateful to Boris Shraiman and the Bilder lab, especially Justin Crest, for helpful discussions. We also acknowledge Lin Yuan, who first documented stage 2 follicle rotation. We thank the TRiP at Harvard Medical School (NIH/NIGMS R01-GM084947) and the Bloomington Stock Center for providing transgenic RNAi fly stocks used in this study. KRL is an American Heart Association graduate fellow. This work was supported by NIH RO1 GM068675 to DB.

Author Contributions

DYC, KRL, and YD conducted the experiments; SJS developed analytical tools; DYC, KRL, and DB designed the experiments and wrote the paper.

EXPERIMENTAL PROCEDURES

RNAi-mediated depletion in follicle cells used a Gal4 insertion in *tj* (Hayashi et al., 2002; Li et al., 2003) with *UAS-RNAi* transgenes. Conditional depletion was carried out in combination with *tubGAL80ts*, using 18º as restrictive temperature and 29º as permissive temperature. Live follicles were cultured *ex vivo* under previously described conditions (Haigo and Bilder, 2011), and imaged on a Zeiss 700 confocal microscope. EB1-GFP comets were analyzed using Fiji (Schindelin et al., 2012). ImSAnE analysis was executed on full stacks of confocal sections, and nematic order was analyzed as described in **Supplemental Experimental Procedures**, where additional genetic and imaging details are provided.

FIGURE LEGENDS

Figure 1. PCP rotation initiates during follicle budding. (A) Stills (opacity projections) from live imaging of germarium through stage 4 follicles, with angular velocity (ω) of each given above. His2AV-mRFP (red) and Vkg-GFP (green) show nuclei and basement membrane respectively; colored dots mark tracked nuclei. The st. 1 follicle initially does not rotate, but between 72 and 132 minutes transitions to st. 2 and begins rotation **(B, C)** Maximum linear and angular velocity of rotating follicles (n>5 for each stage, bars represent SEM). Color-coded bar indicates relative time length of stages of oogenesis. **(D)** BM closure during st. 1-2 transition, shown in single confocal section from live imaging. In the non-rotating st. 1 follicle, BM at the anterior is non-continuous (arrowheads). Rotation initiates after BM becomes continuous around the entire follicle. **(E, F)** Quantitation of relationship between BM completion and follicle rotation (n=11, bars represent SEM).

Figure 2. Germarial PCP revealed by 'unrolling' algorithm. (A) Phalloidin-stained st. 6 follicle, shown in (A) single confocal section at basal surface, (A') maximum intensity projection of confocal stack, and (A'') 3D opacity projections. **(B)** Diagram of ImSAnE unrolling of the basal surface of the follicle. **(C)** ImSAnE unrolling of stage 6 follicle stained with phalloidin and (C') anti-acTub. Nematic order parameters (quantitated in upper left) demonstrate PCP organization. **(D)** Confocal cross-section of germarium stained with phalloidin (red) and anti-acTub (green). **(E)** ImSAnE unrolling of region 2b through stage 3 basal surface of ovariole in D**. (F)** Nematic order quantitation of MTs demonstrate dynamics of PCP organization in the germarium and early follicle. Data for Actin and acetylated Tubulin is shown to the immediate left and right (respectively) of each stage. Scale bars: 10μm.

Figure 3. PCP MTs in the germarium direct rotation. (A) ImSAnE unrolling of basal surface of *CLASP*-depleted ovariole, showing regions 2b through st. 3 stained with phalloidin and anti-acTub. **(B)** Nematic order shows intact actin alignment when MTs are disrupted. (n≥5 for each stages, **p<0.01) **(C, D)** Control stage 9 follicle and mature eggs are elongated, while *CLASP-RNAi* stage 9 follicles and mature eggs are round. **(E)** Rotation speeds of st. 6-7 follicles, depleted at specified times using *tj> CLASP RNAi tubGAL80ts*, or treated with the MT polymerization inhibitor colchicine or the Arp2/3 inhibitor CK-666. **(F)** Quantitation of *tj> CLASP RNAi tubGAL80ts* egg shape.

Figure 4. Fat2 regulates rotation initiation and MT chirality. (A) ImSAnE unrolling of basal surface of *fat2*-depleted ovariole, showing regions 2b through st. 3 stained with phalloidin and anti-acTub. **(B)** Nematic order shows MT and actin alignment resemble WT until st. 2, but become disrupted following st. 3. **(C)** Rotation speeds at st. 7-8 of follicles depleted of *fat2* by RNAi at specified stages. Follicles depleted of *fat2* either prior to or following st. 3 fail to rotate. (**D**) Aspect ratios of eggs from conditional depletion of *fat2*, showing strong early and late requirements for egg shape. (**E**) Egg shapes from *fat2-RNAi-mild* genetic interaction tests. Heterozygosity for either *fat2* or *CLASP* enhances the round egg phenotype. **(F)** Still frame from live imaging of MT +end growth in WT st. 1 follicle. **(G)** Quantification of EB1 growth bias in WT and *fat2*-depleted st. 1 follicle (0=unbiased direction of growth, 1=fully concordant direction of growth), shows that significant MT growth bias in WT is lost when *fat2* is depleted. **(H)** Population-level MT growth biases at st. 1 and follicle rotation directions at st. 6 show similar proportions of chiralities. **(I)** Live imaging of EB1-GFP expressing follicles during st.1 to st. 2 transition reveals rotation with a chirality opposite to that of MT growth bias.

SUPPLEMENTARY FIGURES AND FILES

Supplemental Experimental Procedures and Figures (separate file)

REFERENCES

Bastock, R., and Strutt, D. (2007). The planar polarity pathway promotes coordinated cell migration during Drosophila oogenesis. Development *134*, 3055–3064.

Bilder, D., and Haigo, S.L. (2012). Expanding the morphogenetic repertoire: perspectives from the Drosophila egg. Dev Cell *22*, 12–23.

Cetera, M., and Horne-Badovinac, S. (2015). Round and round gets you somewhere: collective cell migration and planar polarity in elongating Drosophila egg chambers. Curr. Opin. Genet. Dev. *32*, 10–15.

Cetera, M., Ramirez-San Juan, G.R., Oakes, P.W., Lewellyn, L., Fairchild, M.J., Tanentzapf, G., Gardel, M.L., and Horne-Badovinac, S. (2014). Epithelial rotation promotes the global alignment of contractile actin bundles during Drosophila egg chamber elongation. Nature Communications *5*, 5511.

Chen, X.J., Squarr, A.J., Stephan, R., Chen, B., Higgins, T.E., Barry, D.J., Martin, M.C., Rosen, M.K., Bogdan, S., and Way, M. (2014). Ena/VASP proteins cooperate with the WAVE complex to regulate the actin cytoskeleton. Dev Cell *30*, 569–584.

Frydman, H., and Spradling, A. (2001). The receptor-like tyrosine phosphatase lar is required for epithelial planar polarity and for axis determination within drosophila ovarian follicles. Development *128*, 3209–3220.

Galic, M., and Matis, M. (2015). Polarized trafficking provides spatial cues for planar cell polarization within a tissue. Bioessays *37*, 678–686.

Goodrich, L.V., and Strutt, D. (2011). Principles of planar polarity in animal development.

Development *138*, 1877–1892.

Gray, R.S., Roszko, I., and Solnica-Krezel, L. (2011). Planar cell polarity: coordinating morphogenetic cell behaviors with embryonic polarity. Dev Cell *21*, 120–133.

Haigo, S.L., and Bilder, D. (2011). Global tissue revolutions in a morphogenetic movement controlling elongation. Science *331*, 1071–1074.

Harumoto, T., Ito, M., Shimada, Y., Kobayashi, T.J., Ueda, H.R., Lu, B., and Uemura, T. (2010). Atypical cadherins Dachsous and Fat control dynamics of noncentrosomal microtubules in planar cell polarity. Dev Cell *19*, 389–401.

Hayashi, S., Ito, K., Sado, Y., Taniguchi, M., Akimoto, A., Takeuchi, H., Aigaki, T., Matsuzaki, F., Nakagoshi, H., Tanimura, T., et al. (2002). GETDB, a database compiling expression patterns and molecular locations of a collection of Gal4 enhancer traps. Genesis *34*, 58–61.

Heemskerk, I.J., and Streichan, S.J. (2015). Developmental cartography: Compressing Bio-Image Data by Dimensional Reduction. Nature Methods.

Lerner, D.W., McCoy, D., Isabella, A.J., Mahowald, A.P., Gerlach, G.F., Chaudhry, T.A., and Horne-Badovinac, S. (2013). A Rab10-Dependent Mechanism for Polarized Basement Membrane Secretion during Organ Morphogenesis. Dev Cell *24*, 159–168.

Lewellyn, L., Cetera, M., and Horne-Badovinac, S. (2013). Misshapen decreases integrin levels to promote epithelial motility and planar polarity in Drosophila. J. Cell Biol. *200*, 721–729.

Li, M.A., Alls, J.D., Avancini, R.M., Koo, K., and Godt, D. (2003). The large Maf factor Traffic Jam controls gonad morphogenesis in Drosophila. Nat. Cell Biol. *5*, 994–1000.

Matis, M., Russler-Germain, D.A., Hu, Q., Tomlin, C.J., and Axelrod, J.D. (2014). Microtubules provide directional information for core PCP function. eLife *3*, e02893.

Moeller, M.J., Soofi, A., Braun, G.S., Li, X., Watzl, C., Kriz, W., and Holzman, L.B. (2004). Protocadherin FAT1 binds Ena/VASP proteins and is necessary for actin dynamics and cell polarization. Embo J. *23*, 3769–3779.

Nystul, T.G., and Spradling, A. (2010). Regulation of epithelial stem cell replacement and follicle formation in the Drosophila ovary. Genetics *184*, 503–515.

Olofsson, J., Sharp, K.A., Matis, M., Cho, B., and Axelrod, J.D. (2014). Prickle/spiny-legs isoforms control the polarity of the apical microtubule network in planar cell polarity. Development *141*, 2866–2874.

Schindelin, J., Arganda-Carreras, I., Frise, E., Kaynig, V., Longair, M., Pietzsch, T., Preibisch, S., Rueden, C., Saalfeld, S., Schmid, B., et al. (2012). Fiji: an open-source platform for biological-image analysis. Nat. Methods *9*, 676–682.

Sepich, D.S., Usmani, M., Pawlicki, S., and Solnica-Krezel, L. (2011). Wnt/PCP signaling controls intracellular position of MTOCs during gastrulation convergence and extension

movements. Development *138*, 543–552.

Shimada, Y., Yonemura, S., Ohkura, H., Strutt, D., and Uemura, T. (2006). Polarized transport of Frizzled along the planar microtubule arrays in Drosophila wing epithelium. Dev Cell *10*, 209–222.

Singh, J., and Mlodzik, M. (2012). Planar cell polarity signaling: coordination of cellular orientation across tissues. Wiley Interdiscip Rev Dev Biol *1*, 479–499.

Spradling, A.C. (1993). Oogenesis. In The Development ofDrosophila Melanogaster, C.M.A.M.-A.A. Bate, ed. (Cold Spring Harbor: Cold Spring Harbor Press).

Squarr, A.J., Brinkmann, K., Chen, B., Steinbacher, T., Ebnet, K., Rosen, M.K., and Bogdan, S. (2016). Fat2 acts through the WAVE regulatory complex to drive collective cell migration during tissue rotation. J. Cell Biol. *212*, 591–603.

Tanoue, T., and Takeichi, M. (2004). Mammalian Fat1 cadherin regulates actin dynamics and cell-cell contact. J. Cell Biol. *165*, 517–528.

Viktorinova, I., Konig, T., Schlichting, K., and Dahmann, C. (2009). The cadherin Fat2 is required for planar cell polarity in the Drosophila ovary. Development *136*, 4123–4132.

Viktorinova, I., Pismen, L.M., Aigouy, B., and Dahmann, C. (2011). Modelling planar polarity of epithelia: the role of signal relay in collective cell polarization. J R Soc Interface.

Viktorinová, I., and Dahmann, C. (2013). Microtubule polarity predicts direction of egg chamber rotation in Drosophila. Current Biology *23*, 1472–1477.

Vladar, E.K., Antic, D., and Axelrod, J.D. (2009). Planar Cell Polarity Signaling: The Developing Cell's Compass. Csh Perspect Biol *1*, a00296.

Wallingford, J.B. (2012). Planar cell polarity and the developmental control of cell behavior in vertebrate embryos. Annu. Rev. Cell Dev. Biol. *28*, 627–653.

Zallen, J.A. (2007). Planar polarity and tissue morphogenesis. Cell *129*, 1051–1063.

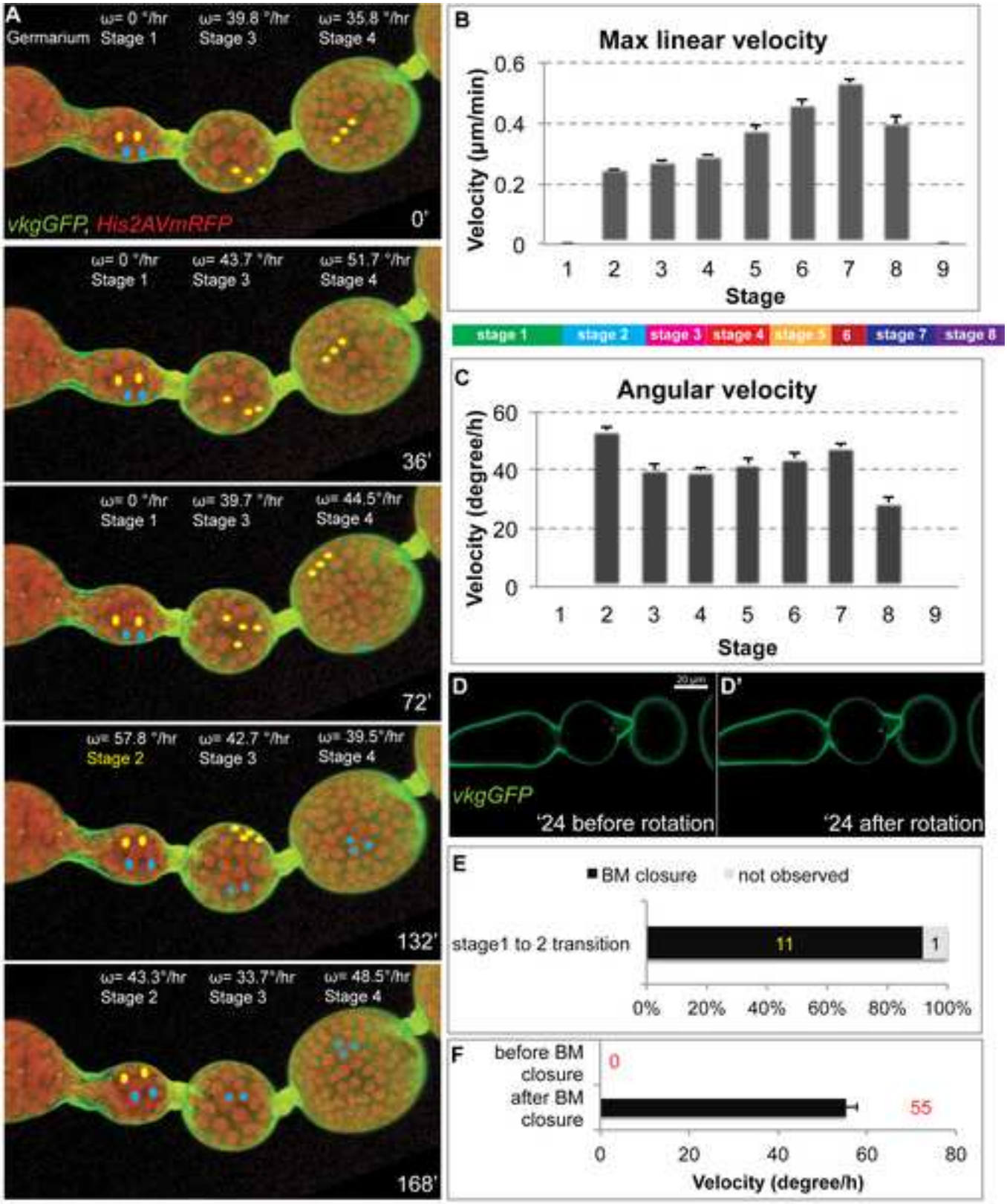

Fig.1

Figure 2

Click here to download Figure FIG2.tif

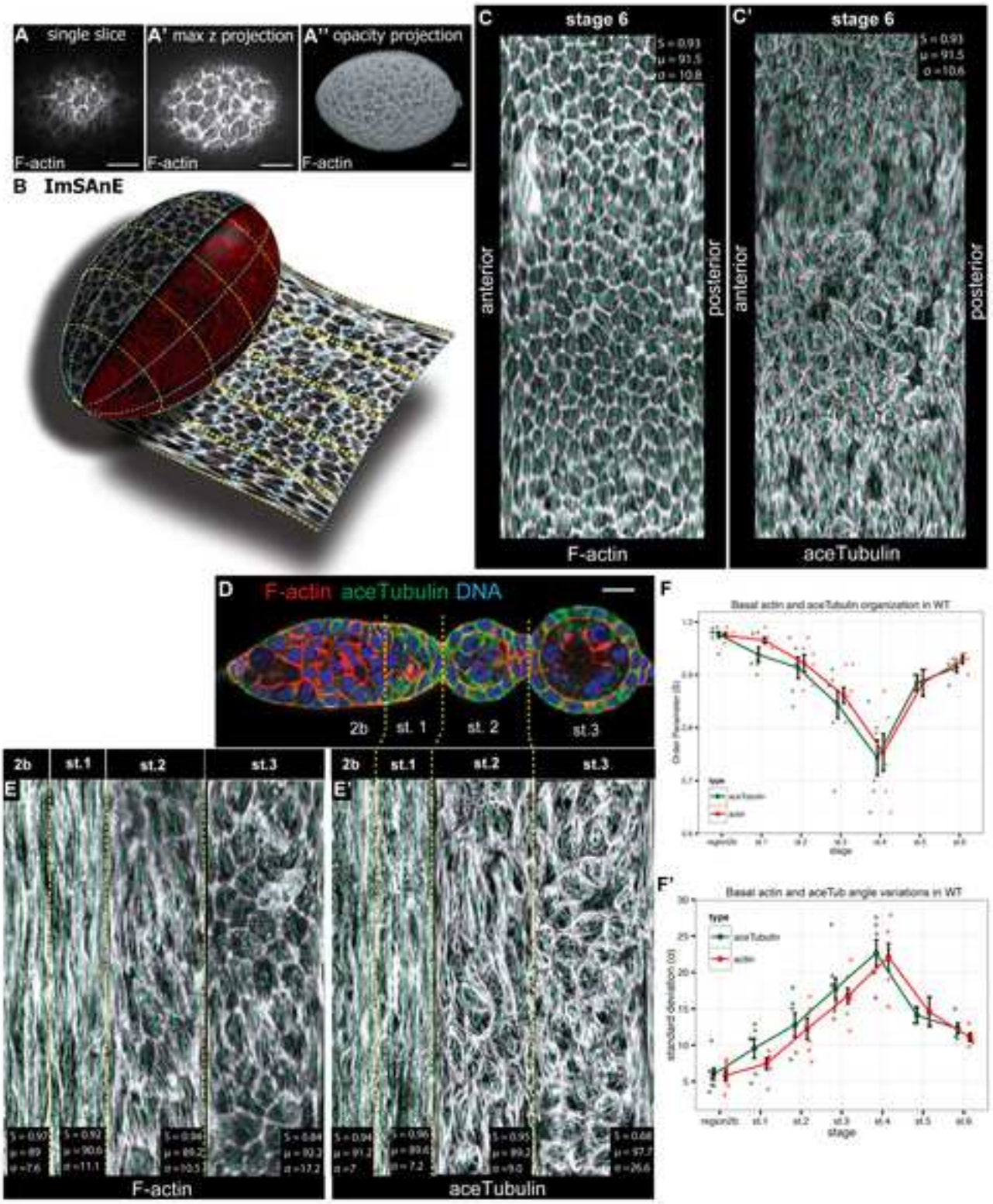

Figure 2

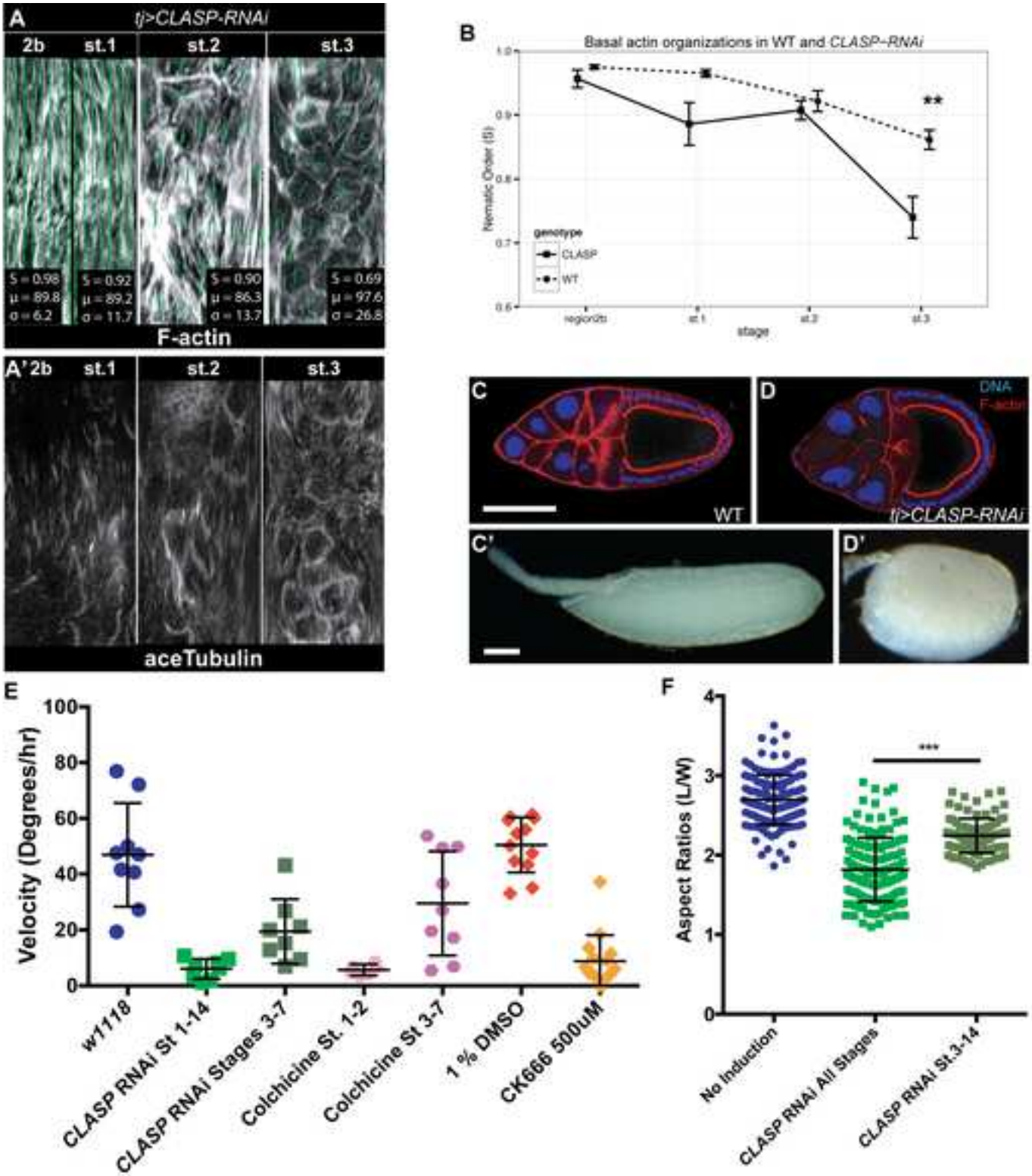

Figure 3

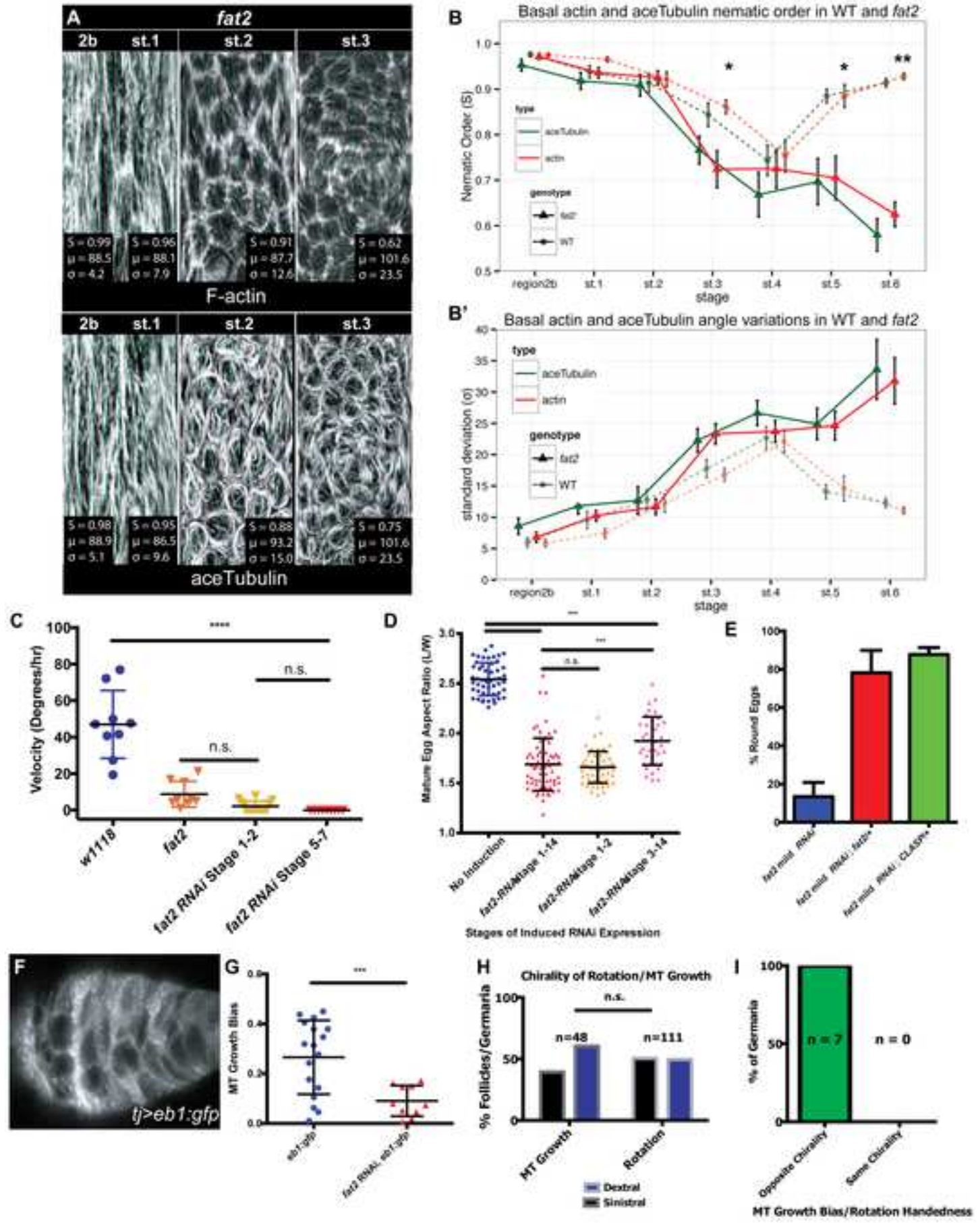

Figure 4

SUPPLEMENTAL EXPERIMENTAL PROCEDURES

Fly Strains, culture, and drug treatments

All flies were maintained at 25°C unless otherwise indicated. *fat2*^{58D} and *fat2*^{103C} are gifts from Dr. Christian Dahmann. *UAS-EB1::GFP* is a gift from Nasser Rusan, and *UAS-SpastinEP* is a gift from Nina Tang Sherwood. RNAi strains against the following genes were generated by the Harvard TRiP: *Fat2* (BDSC #40888), *CLASP* (BDSC #34669), *Hem* (BDSC #29406), *Abi (*BDSC #51455*); mCherry* (BDSC #35785) was used as a control. Mild *Fat2* knockdown was achieved using VDRC ID #27113. To temporally control knockdown, *tj-GAL4 tubP-GAL80*^{ts} was crossed to *UAS*-RNAi strains. Adult females were collected at 22° and shifted to 29°. Stage-specific temperature shifts were timed based on duration of stages of ovarian development (Spradling, 1993), informed by the temperature dependence of Drosophila development. To depolymerize microtubules, adult flies were fed with yeast paste mixed with colchicine at 62.5 μg/ml (Sigma); to inhibit Arp2/3 activity, cultured ovarioles were treated with CK-666 at 500 μg/ml (Millipore). All flies were flipped onto fresh yeast daily to ensure no mid-stage follicle degeneration or egg retention.

Microscopy and Immunostaining

Ex vivo follicle culture was performed as previously described (Haigo and Bilder, 2011; Spradling, 1993), with minor modifications. Images were acquired using an inverted Zeiss LSM700 with LD C-Apochromat 40x/NA 1.1 water-immersion lens. Other fluorescent images were acquired with a Zeiss LSM700 using Plan-Apochromat 40x/ NA 1.3 oil-immersion lens. Follicle and egg aspect ratios were calculated from images taken with an AxioImager.M1 (Zeiss) with 10x/NA 0.3 air objective lens; data was analyzed and displayed using GraphPad Prism 6 or Rstudio(Team, 2015) with ggplot2. Figures were assembled in Adobe Illustrator CS6.

Adult ovaries were dissected in PBS or Schneider's Drosophila medium (Gibco) and fixed with 4% formaldehyde in PBS for 15 min and stained as previously described. Stains with TRITC-phalloidin (Sigma) and DAPI (Molecular Probes) were mounted in SlowFade Antifade solution (Invitrogen). The following antibodies were also used: mouse monoclonal anti-acetylated-α-tubulin (1:300, Santa Cruz), and AlexaFluor-488, -563, and -633 conjugated secondary antibodies (1:400, Molecular Probes).

Image analyses and statistics

Follicle rotation velocities were either measured by the displacement of cell nuclei perpendicular to the AP axis, taken at the follicle equator, or plasma membranes stained with 5μg/mL FM4-64FX dye (Molecular Probes). Angular velocity was calculated using measured follicle maximal circumference. 3D Opacity projections were generated with Volocity (Perkin Elmer). Other images were processed in Fiji (Schindelin et al., 2012).

Orientation and alignment of the cytoskeleton was analyzed in fixed ovarioles stained with TRITC-phalloidin and anti-acetylated-tubulin, mounted on concave slides (Ted Pella) to prevent deformation. *in toto* images were collected with confocal microscopy with pixel width of 0.07-0.15 μm and voxel depth of 0.35-0.50 μm.

We used ImSAnE (Heemskerk and Streichan, 2015) to ‘unroll’ follicles and germaria. In brief, coarse identification of the Surface Of Interest (SOI) is followed by representing the SOI as a smooth mesh, equipped with a coordinate system for mapping to the plane. Images were first rescaled to uniform aspect ratio at the most fine resolution. The ovariole SOI was identified using the basal F-actin signal and the ‘ilastik’ (Sommer et al., 2011) segmentor interface implemented in ImSAnE, which produced a coarse point cloud. Meshlab (Cignoni et al., 2008) generated a smooth triangulation of

the basal actin layer from the point cloud, following publicly available ImSAnE protocols. The ImSAnE CylinderMeshWrapper class automatically generates a coordinate system embedded in the triangulation for mapping the SOI to the plane: the long axis and azimuth around it are used as a discretized coordinate pair on the surface and the image data interpolated at the corresponding embedding point of each discretized coordinate pixel, generating a planar projection of the data. Image contrast was enhanced with the contrast limited adaptive histogram enhancement (CLAHE) plugin (Fiji). To automatically determine local orientation of actin filaments, region 2 germaria and stage 1 follicles were first screened with a uniform raster of 20x20 px/4 μm^2, overlapping by 2.23 µm; for stage 2 and older, cells were segmented based on cortical actin signal. To determine the polarization axis of basal actin filaments A in boxes or segmented cells, we measured spatial frequency patterns using Fourier's method, from which a nematic order parameter defined as $S = 1/N \sum_{k=1}^{N} e^{2iA}$ was constructed. Orientation to the A-P axis (defined by polar cell position in early follicles, and long axis in germaria and elongated follicles) and the standard deviation (σ) of angles within a follicle were measured using the curvature-corrected dot product of unit vectors with corresponding orientation. Error bars in cytoskeletal alignment analyses represents SEM and statistical significance was assessed by Welch's unequal variances *t*-test. Error bars in charts for rotation velocity (Figure3E, 4C), mature egg aspect ratio (Figure3F, 4D), percentage round eggs (Figure 4E) represent standard deviation. Unless stated otherwise, statistical significance was assessed by Welch's unequal variances *t*-test.

EB1-GFP comet tracking

tj>UAS-EB1:GFP flies were raised on yeast for 5 days at 29° C, flipped onto fresh yeast for 6-12 hours. Ovarioles were dissected in modified Schneider's medium and mounted using low-melting point agar. Movies of basal EB1 comet growth were made on the Zeiss LSM700 with LD C-Apochromat 40x/NA 1.1 water-immersion lens. Individual EB1 comets were tracked manually in Fiji by generating kymographs perpendicular to the AP axis of the germarium and measuring the slope of EB1:GFP comet growth. Microtubule growth bias was calculated by the formula |(D-S)/T| where D equals the number of dextral comets, S equals the number of sinistral comets and T is the total number of comets. Statistical significance was assessed by Unpaired T-test.

SUPPLEMENTAL FIGURE LEGENDS

Supplemental Fig. 1: Early stages of follicle development (related to Fig. 1)
(A) Confocal section of anterior ovariole, stained for DNA (blue), F-actin (red) and acetylated tubulin (green). **(B)** Diagram of germarium and st. 2 follicle, showing position of stem cells, somatic and germline cells, and stalk cells.

Supplemental Fig. 2: Arp2/3 regulators are required for egg elongation (related to Fig. 3)
Knockdown of Arp2/3 regulators *Hem* **(A)** and *Abi* **(B)** by *tjGAL4 UAS-RNAi* in genetic screen produces round eggs; aspect ratios are quantitated in **(C)**.

Supplemental Fig. 3: Characterization of *fat2 RNAi* phenotype (related to Fig. 4)
(A) Aspect ratio and **(B)** st. 7 actin alignment of *fat2* null mutant vs *tj>fat2 RNAi* follicles demonstrates effective depletion of *fat2* function by RNAi.

Supplemental Movie S1, related to Fig. 1: Live imaging of ovariole (genotype: *vkgGFP, His2aVmRFP*) shows rotation commencing as follicle buds at st. 2.

Supplemental Movie S2, related to Fig. 4: Live imaging of *fat2*-depeleted ovariole (genotype:*tj>fat2 RNAi; vkgGFP, His2aVmRFP*) shows failure to initiate rotation.

Supplemental Movie S3, related to Fig. 4: EB1-GFP comet imaging in the germarium.

Supplemental Movie S4, related to Fig. 4: Imaging of EB1-GFP stage 1-2 follicle during the initiation of rotation. MT growth bias for this follicle is 0.48 sinistral at st 1.

SUPPLEMENTAL REFERENCES

Cignoni, P., Callieri, M., Corsini, M., Dellepiane, M., Ganovelli, F., and Ranzuglia, G. (2008). MeshLab: an Open-Source Mesh Processing Tool. Eurographics Italian Chapter Conference.

Haigo, S.L., and Bilder, D. (2011). Global tissue revolutions in a morphogenetic movement controlling elongation. Science *331*, 1071–1074.

Heemskerk, I.J., and Streichan, S.J. (2015). Developmental cartography: Compressing Bio-Image Data by Dimensional Reduction. Nature Methods.

Schindelin, J., Arganda-Carreras, I., Frise, E., Kaynig, V., Longair, M., Pietzsch, T., Preibisch, S., Rueden, C., Saalfeld, S., Schmid, B., et al. (2012). Fiji: an open-source platform for biological-image analysis. Nat. Methods *9*, 676–682.

Sommer, C., Straehle, C., Kothe, U., and Hamprecht, F.A. (2011). ilastik: Interactive Learning and Segmentation Toolkit. pp. 230–233.

Spradling, A.C. (1993). Developmental genetics of oogenesis. In The Development of Drosophila Melanogaster, M. Bate, and A. Martinez Arias, eds. (New York: CSHL Press), pp. 1–70.

R Team (2015). RStudio: Integrated Development for R. Www.Rstudio.com.

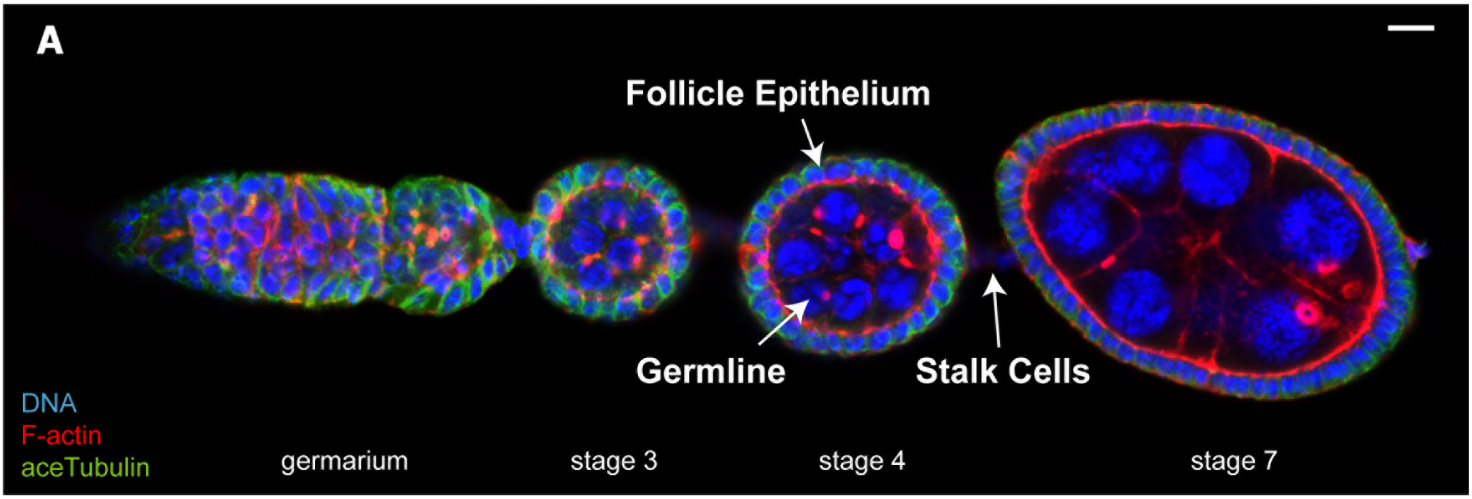

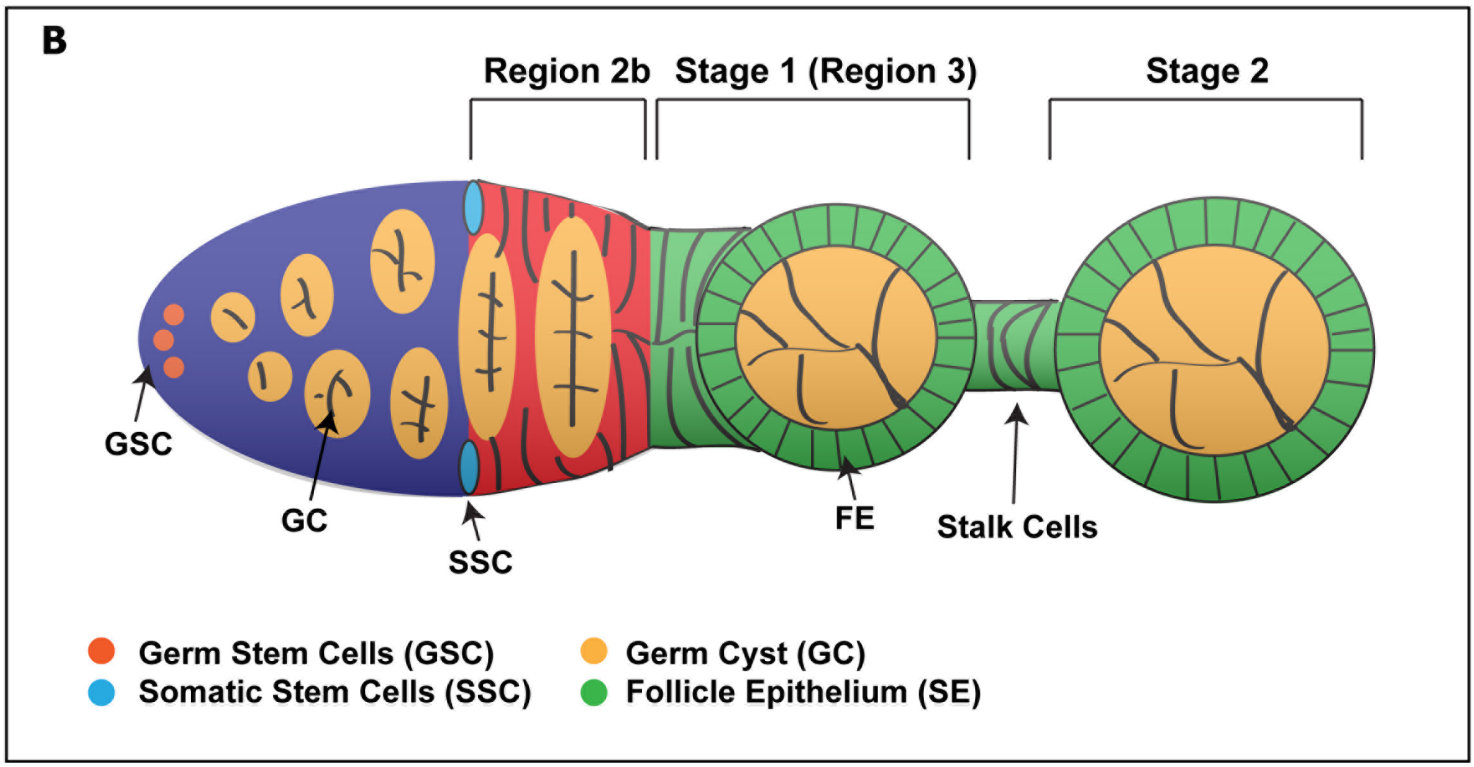

Supplemental Figure 1

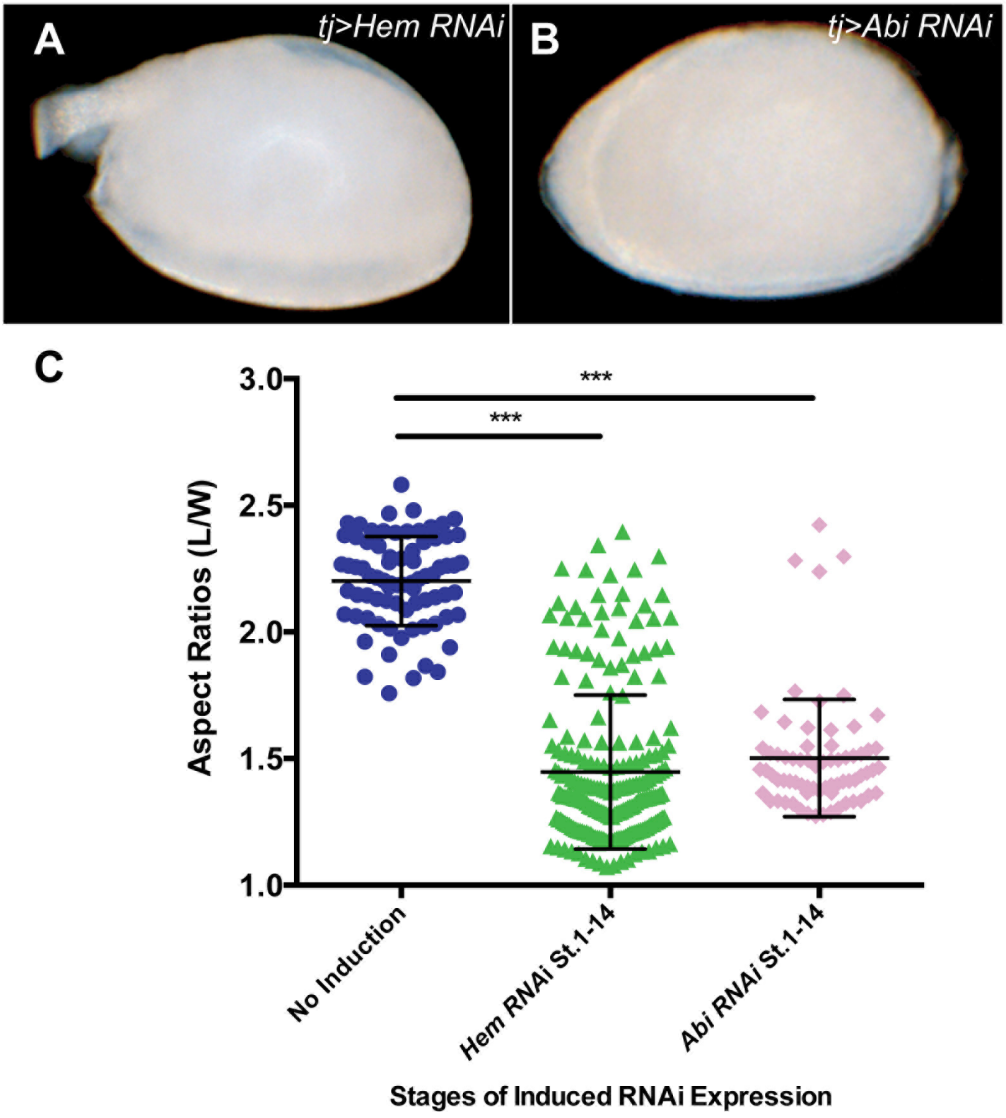

Supplemental Figure 2

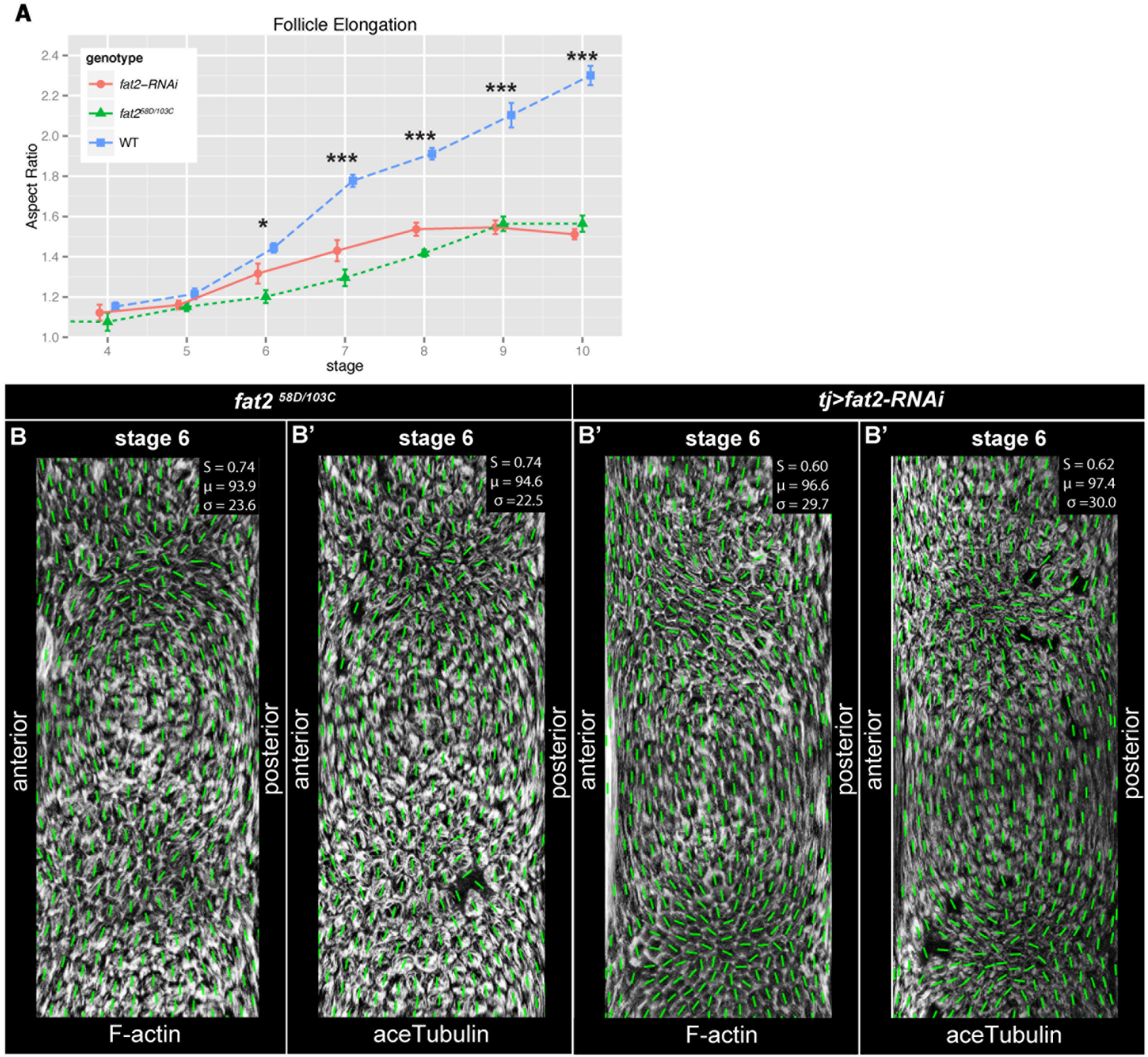

Supplemental Figure 3

Supplemental Movie 1

Click here to access/download

Supplemental Movies & Spreadsheets

SUPPMOV-1.avi

Supplemental Movie 2

Click here to access/download

Supplemental Movies & Spreadsheets

SUPPMOV-2.mov

Supplemental Movie 3

Click here to access/download

Supplemental Movies & Spreadsheets

SUPPMOV-3.avi

Supplemental Movie 4

Click here to access/download

Supplemental Movies & Spreadsheets

SUPPMOV-4.avi

SUPPLEMENTAL INFORMATION INVENTORY